Spectrochimica Acta Part A 81 (2011) 754–763

Contents lists available at ScienceDirect

Spectrochimica Acta Part A: Molecular and Biomolecular Spectroscopy

journal homepage: www.elsevier.com/locate/saa

# 2-[(1H-Benzimidazol-2-ylmethyl)-amino]-benzoic acid methyl ester: Crystal structure, DFT calculations and biological activity evaluation

Nour T. Abdel Ghani*, Ahmed M. Mansour

*Chemistry Department, Faculty of Science, Cairo University, Gamaa Street, Giza 12613, Egypt*

ARTICLE INFO

*Article history:*
Received 14 May 2011
Received in revised form 27 June 2011
Accepted 3 July 2011

*Keywords:*
Benzimidazole
GIAO NMR
NBO
Antibacterial

ABSTRACT

In the present study, structural properties of 2-[(1H-benzimidazol-2-ylmethyl)-amino]-benzoic acid methyl ester have been studied extensively by spectral methods and X-ray crystallography. Quantum mechanical calculations of energies, geometries, vibrational wavenumbers, NMR and electronic transitions were carried out by DFT using B3LYP functional combined with 6-31G(d) basis set. Natural bond orbitals (NBO) analysis and frontier molecular orbitals were performed at the same level of theory. DFT calculations showed good agreement between the theoretical and experimental values of optimized and X-ray structure as well as between the vibrational and NMR spectroscopy. The title compound was screened for its antibacterial activity referring to *Tetracycline* as standard antibacterial agent.



## 1. Introduction

Owing to their parasitic and antiviral activities, benzimidazole and its derivatives were widely investigated in medical and industrial fields. Benzimidazole as its 5,6-dimethyl derivative is present in vitamin $B_{12}$ and related biomolecules [1]. In addition, benzimidazole derivatives have found wide use as antihelmintic [2], antitumor [3], and antimicrobial agents [4]. Moreover, benzimidazoles can be used in liquid crystals [5], OLED's [6], switch's devices [7], and DNA intercalator [3]. A considerable number of metal benzimidazole complexes including Cr–Zn, Pd, Pt, Au, and Re were studied [5,8,9]. Benzimidazole is also of interest as a corrosion inhibitor for metals and alloys (benzimidazole molecule shows two anchoring sites suitable for surface bonding: the nitrogen atom with its lonely $sp^2$ electron pair and the aromatic ring). The molecular structure and anticorrosion mechanism have been previously studied [10]. The biological activities of some other related benzimidazole derivatives e.g. (1H-benzimidazol-2-ylmethyl)-(4-nitro-phenyl)-amine concerning the antibacterial, antitumor activity, structure–activity relationship and a comparison with cis-platin have been recently reported [9,11]. The results showed that the antimicrobial activity is affected by the nature of the substituents of the aniline ring. In the view of these facts, the aim of the present study is to synthesize new benzimidazole containing compound (Fig. 1), which may be used as an antimicrobial substance, and characterize it by X-ray crystallography, FT-IR, $^1$H, $^{13}$C NMR, UV/vis., and elemental analysis. In addition, structural optimization by DFT calculations was performed and the results were compared with X-ray data and simulated vibrational and NMR spectra.

## 2. Experimental

### 2.1. Synthesis

All chemicals used in the preparation and investigation of the present study were of reagent grade (Sigma). The benzimidazole derivative was prepared by condensation of equimolar quantities of 2-chloromethylbenzimidazole [12] with 2-amino-benzoic acid methyl ester in ethanol in presence of small amount of sodium iodide for about 18 h. Then, the reaction mixture was neutralized and the solid was separated by cooling, and re-crystallized from ethanol. The 2-[(1H-benzimidazol-2-yl-methyl)-amino]-benzoic acid methyl ester was obtained as yellow crystals. Yield 80%; mp $210 \pm 1\,^{\circ}$C; mass spectrum produced by electron impact (EI) ionization showed $m/z$: 281 ($M^+$) (calcd. 281.31), 248, 220, 131 and 118. Anal. Calc. for $C_{16}H_{15}N_3O_2$: %C, 68.31; %H, 5.37; %N, 14.94. Found: %C, 67.94; %H, 5.00; %N, 14.80.

### 2.2. Instruments

Infrared spectrum was recorded as KBr pellet using *FTIR-460 plus*, *JASCO*, in 4000–200 $cm^{-1}$ region. The $^1$H and $^{13}$C NMR spectra were run at 300 MHz in DMSO-$d_6$ using *Varian-Oxford Mercury VX-300 NMR*. Elemental microanalyses were performed at the Micro-analytical Center, Cairo University. The analyses were

* Corresponding author. Tel.: +20 2 0106700375; fax: +20 2 35728843.
*E-mail address:* noureta2002@yahoo.com (N. T. Abdel-Ghani).

1386-1425/$ – see front matter © 2011 Elsevier B.V. All rights reserved.
doi:10.1016/j.saa.2011.07.021

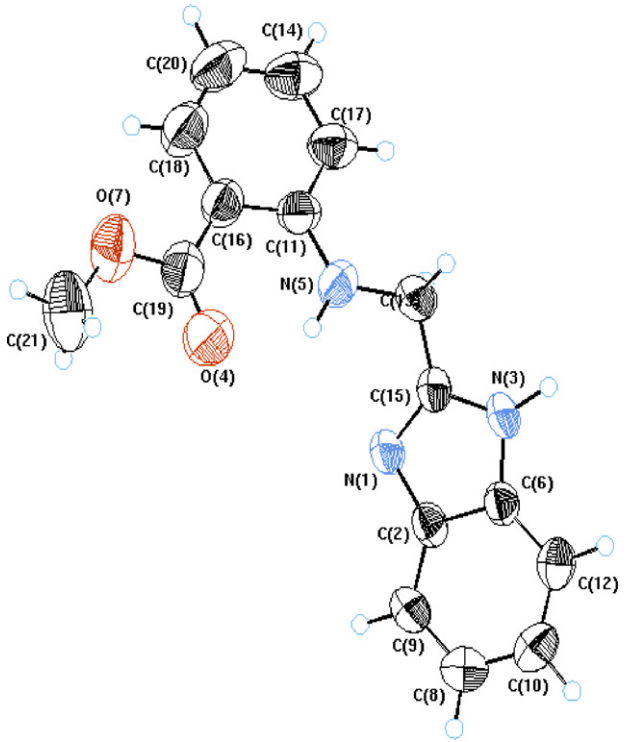


**Fig. 1.** ORTEP plot of 2-[(1H-benzimidazol-2-yl-methyl)-amino]-benzoic acid methyl ester.

repeated twice to check the accuracy of the analyzed data. The mass spectrum was recorded by the aid of a *SHIMADZU QP-2010 plus mass spectrometer* at 70 eV. The UV/vis. measurements were carried out using automated spectrophotometer UV/vis. *SHIMADZU Lambda 4B* using 1 cm matched quartz cells.

### 2.3. Computational calculations

The molecular structure of the title compound in the ground state was optimized by a DFT method using B3LYP functional [13] combined with 6-31G(d) basis set. The starting geometry for DFT calculations was constructed based on crystallographic data without any symmetry restriction. Calculations were carried out using *GAUSSIAN 03* [14] suite of programs. The vibrational frequencies and the corresponding normal modes were evaluated at the optimized geometry [13]. Vibrational modes were analyzed using GAUSSVIEW software [15]. The NMR chemical shifts were computed at the B3LYP/6-311 + G(2d,p) level of theory in the gaseous state by applying GIAO approach [16] and the values for the $^{1}H$, $^{13}C$ isotropic were referenced to TMS, which was calculated at the same level of theory. The effect of solvents (DMSO, $H_2O$, and $CHCl_3$) on the theoretical NMR parameters was performed using the default IEF–PCM model provided by GAUSSIAN 03. Natural bond orbitals (NBO) analysis and frontier molecular orbitals were performed at the same level of theory.

### 2.4. X-ray crystallography

The crystallographic analysis was carried out on an Enraf–Nonius CAD4 diffractometer, using graphite monochromated Mo-$K_\alpha$ radiation ($k$ = 0.71069 Å) at room temperature. Three standard reflections were monitored during data collection and no significant intensity decay was observed. All diffracted intensities were corrected for Lorentz and polarization effects [17,18]. The structure was solved by direct methods and was refined by the full-matrix least-squares method using *SIR*92 [19] computer programs in the space group $P2_1/c$. All diagrams and calculations were performed using maXus [20], while the molecular graphics were given using *ORTEP* [21]. The figures involving Hydrogen-bonds and packing were drawn using Mercury [21]. Further relevant crystallographic data are summarized in Supplementary Material, Table S1.

### 2.5. Biological activity studies

The antimicrobial activity of the test sample was determined using a modified Kirby-Bauer disc diffusion method [22] under standard conditions using *Mueller-Hinton* agar medium, as described by NCCLS [23]. The antimicrobial activities were carried out using culture of *B. subtilis*, *S. aureus*, and *S. faecalis* as Gram-positive bacteria and *E. coli*, *P. aeruginosa*, and *N. gonorrhoeae* as Gram-negative bacteria. Briefly, 100 μL of the test bacteria were grown in 10 mL of fresh media until they reached a count of approximately 108 cells/mL. 100 μL of microbial suspension was spread onto agar plates corresponding to the broth in which they were maintained. DMSO (0.1 mL) alone was used as control under the same conditions for each microorganism, subtracting the diameter of inhibition zone resulting with DMSO, from that obtained in each case. The antimicrobial activities could be calculated as a mean of three replicates. The results were compared with a similar run of *Tetracycline* as an antibacterial.

## 3. Results and discussion

### 3.1. X-ray crystallography

A view of the molecular structure of the benzimidazole compound is shown in Fig. 1 and its selected crystallographic data are presented in Table 1. This compound crystallizes in a monoclinic space group $P2_1/c$. The cell packing is shown in Supplementary Material, Fig. S1. The crystal structure is deviated from the planarity, where the dihedral angle (N1–C15–C13–N5) between the benzimidazole ring and the aniline moiety is 36°. This deviation is possibly caused by the intermolecular hydrogen bonding, N3–H. . .N1 with donor–acceptor distance of 1.936 Å. The title compound forms an infinite chain structure through the intermolecular hydrogen along the "b" axis as shown in Fig. 2. In addition, a six-membered ring is formed by the intramolecular hydrogen bond between the secondary amino group and the carbonyl group in the ortho position (Fig. 2). The N5–H. . .O4 (D–A) distance is 2.678 (3) Å and the DHA angle is 131.5°. The bond length of C19=O4 group is 1.216 (2) Å. A significant difference (0.034 Å) is found between the bond lengths N1–C15 and N3–C15. This confirms that the hydrogen atom is fixed at one of the two nitrogen atoms through the intermolecular hydrogen bonding. It is possible to observe the π–π stacking interactions along the "b" crystallographic axis, as evidenced by the distance of ca. 3.4 Å between the ring planes.

### 3.2. DFT studies

#### 3.2.1. Geometry optimization

Full geometry optimization of the title compound was performed at the DFT level of theory [13]. As shown in Table 1, the relative errors in the calculated values are less than 2%. Most of the optimized bond lengths are slightly longer than the experimental values agreeing within 0.007–0.026 Å except for N–C bonds (0.059 Å), while the bond angles are slightly different by 0.2–2.2° except N–C–C angle (4.6°). This happens because the calculations were performed in gaseous state, whereas packing molecules with inter- and intramolecular interactions are treated in the experimental measurements. Owing to the low scattering factors of

**Table 1**
Selected experimental and calculated geometry parameters for 2-[(1H-benzimidazol-2-yl-methyl)-amino]-benzoic acid methyl ester.

| Bond lengths (Å) | Exp. | Calcd. | Bond angles (°) | Exp. | Calcd. | Charges ($e$) |
|---|---|---|---|---|---|---|
| N1C2 | 1.394 | 1.390 | C2N1C15 | 103.9 | 105.2 | N1 = −0.498 |
| N1C15 | 1.319 | 1.307 | N1C2C6 | 110.6 | 110.2 | C2 = 0.113 |
| C2C6 | 1.385 | 1.415 | N1C2C9 | 129.5 | 129.8 | N3 = −0.578 |
| C2C9 | 1.396 | 1.399 | C6C2C9 | 119.8 | 119.8 | O4 = −0.628 |
| N3C6 | 1.386 | 1.387 | C6N3C15 | 106.8 | 107.0 | N5 = −0.611 |
| N3C15 | 1.353 | 1.378 | C11N5C13 | 124.5 | 123.3 | C6 = 0.124 |
| O4C19 | 1.216 | 1.225 | C2C6N3 | 105.0 | 104.4 | O7 = −0.549 |
| N5C11 | 1.369 | 1.364 | C2C6C12 | 122.7 | 122.5 | C8 = −0.253 |
| N5C13 | 1.434 | 1.438 | N3C6C12 | 132.2 | 133.0 | C9 = −0.221 |
| C6C12 | 1.385 | 1.395 | C19O7C21 | 117.4 | 115.2 | C10 = −0.235 |
| O7C19 | 1.330 | 1.357 | C9C8C10 | 122.1 | 121.3 | C11 = 0.231 |
| O7C21 | 1.448 | 1.434 | C2C9C8 | 117.6 | 117.9 | C12 = −0.268 |
| C8C9 | 1.368 | 1.392 | C8C10C12 | 121.5 | 121.5 | C13 = −0.301 |
| C8C10 | 1.377 | 1.409 | N5C11C16 | 120.3 | 121.7 | C14 = −0.189 |
| C10C12 | 1.386 | 1.394 | N5C11C17 | 122.0 | 120.7 | C15 = 0.418 |
| C11C16 | 1.411 | 1.433 | C16C11C17 | 117.7 | 117.5 | C16 = −0.219 |
| C11C17 | 1.402 | 1.417 | C6C12C10 | 116.2 | 116.6 | C17 = −0.308 |
| C13C15 | 1.490 | 1.502 | N5C13C15 | 109.3 | 110.0 | C18 = −0.171 |
| C14C17 | 1.360 | 1.387 | C17C14C20 | 121.1 | 121.1 | C19 = 0.812 |
| C14C20 | 1.384 | 1.399 | N1C15N3 | 113.6 | 113.1 | C20 = −0.287 |
| C16C18 | 1.400 | 1.405 | N1C15C13 | 124.2 | 125.3 | C21 = −0.320 |
| C16C19 | 1.465 | 1.474 | N3C15C13 | 122.1 | 121.6 | N3H = 0.433 |
| C18C20 | 1.360 | 1.387 | C11C16C18 | 118.7 | 119.5 | N5H = 0.466 |
| N3H3 | 0.960 | 1.009 | C11C16C19 | 121.5 | 120.5 | C9H = 0.248 |
| N5H5 | 0.960 | 1.018 | C18C16C19 | 119.8 | 120.0 | C12H = 0.236 |
| | | | C11C17C14 | 121.6 | 121.3 | C18H = 0.253 |
| | | | C16C18C20 | 122.4 | 121.9 | C20H = 0.236 |
| | | | O4C19O7 | 120.5 | 121.2 | |
| | | | O4C19C16 | 125.8 | 125.6 | |
| | | | O7C19C16 | 113.6 | 113.1 | |
| | | | C14C20C18 | 118.5 | 118.6 | |
| $E$ a.u. | | | −933.439 | | | |
| Zero-point $E$ (kcal mol$^{-1}$) | | | 180.170 | | | |
| Rotational constants (GHz) | | | 0.613, 0.143, 0.116 | | | |
| Entropy (cal mol$^{-1}$ K$^{-1}$) | | | | | | |
| Translational | | | 42.799 | | | |
| Rotational | | | 34.716 | | | |
| Vibrational | | | 63.840 | | | |
| Total dipole moment ($D$) | | | 3.70 | | | |

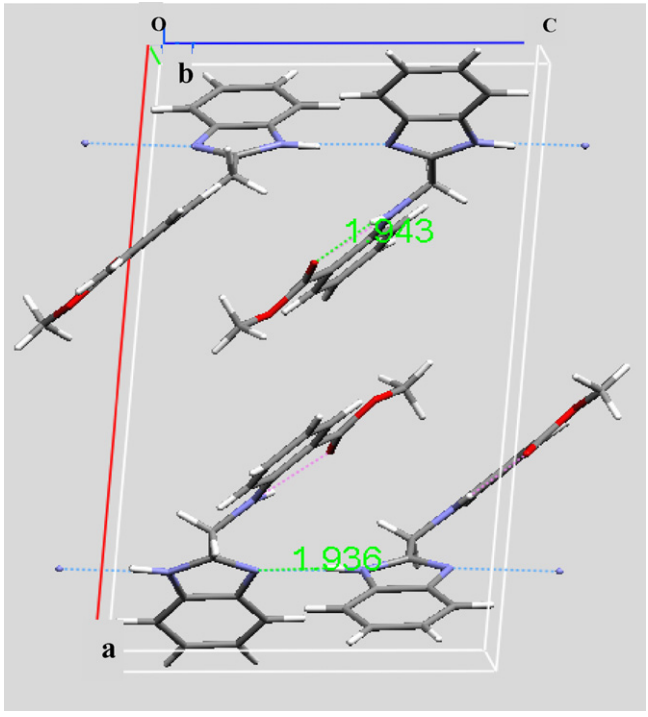


**Fig. 2.** Inter- and intramolecular hydrogen bonding stabilizing the crystal packing of 2-[(1H-benzimidazol-2-yl-methyl)-amino]-benzoic acid methyl ester.

hydrogen atoms in X-ray diffraction, the experimental bond lengths of X–H bonds are expected to be shorter than the estimated bond lengths. This compound shows accumulation of the negative charge density on the pyridine-type nitrogen, which is a very important structural feature related directly to the ability to bind the metal ions. Several calculated thermodynamic parameters are presented in Table 1.

### 3.2.2. *Natural bond orbital (NBO) analysis*

The NBO approach of Weinhold and co-workers [24] has been frequently used in the evaluation of the anomeric effect [25] and the origin of internal rotation barrier [26]. NBO analysis provides an efficient method for studying intra- and intermolecular bonding and interaction among bonds, and provides a convenient basis for investigating charge transfer or conjugative interaction in molecular systems. The hyperconjugative interaction energy was deduced from the second-order perturbation approach [27]. The hyperconjugative interactions are formed by the orbital overlap between σ(C–C) bond orbital to σ*(C–C) anti-bonding orbital, which results in intramolecular charge transfer (ICT) causing stabilization of the system. The larger the second order interaction energy ($E^2$) value, the more intensive is the interaction between electron donors and electron acceptors, i.e. the more donating tendency from electron donors to electron acceptors and the greater the extent of conjugation of the whole system. These interactions can be identified by finding the increase in electron density (ED) in anti-bonding orbital that weakens the respective bonds. NBO analysis has been performed on the molecule at the B3LYP/6-31G(d)

**Table 2**
The most important interactions between "filled" (donors) Lewis-type NBOs and "empty" (acceptors) non-Lewis NBOs.

| Donor[a] Lewis-type NBOs (A–B) | Occupancy | Acceptor[b] non Lewis NBOs | NBOs | $E(2)$ (kJ mol$^{-1}$) | $E(j)-E(i)$[c] ($\times 10^3$ kJ mol$^{-1}$) | $F(i,j)$[d] ($\times 10^3$ kJ mol$^{-1}$) |
|---|---|---|---|---|---|---|
| π(C8–C10) | 1.640 | π*(C2–C9) | 0.022 | 85 | 0.734 | 0.181 |
| π(C8–C10) | 1.640 | π*(C6–C12) | 0.021 | 80 | 0.708 | 0.170 |
| π(C18–C20) | 1.690 | LP C16 | 1.136 | 164 | 0.341 | 0.220 |
| π(C14–C17) | 1.979 | RY* C11 | 0.006 | 214 | 0.367 | 0.246 |
| LP(1)N1 | 1.915 | σ*(N3–C15) | 0.042 | 45 | 2.098 | 0.218 |
| LP(1)N3 | 1.632 | π*(C6–C12) | 0.021 | 158 | 0.786 | 0.254 |
| LP(1)N3 | 1.632 | π*(N1–C15) | 0.333 | 202 | 0.761 | 0.278 |
| LP(1)C16 | 1.136 | π*(C18–C20) | 0.015 | 221 | 0.393 | 0.286 |
| LP(1)C16 | 1.136 | π*(C19–O4) | 0.018 | 298 | 0.315 | 0.281 |
| LP(1)O7 | 1.963 | π*(C19–O4) | 0.018 | 363 | 0.839 | 0.299 |
| LP(1)O4 | 1.968 | σ*(C16–C19) | 0.055 | 197 | 1.888 | 0.249 |
| LP(1)O4 | 1.968 | σ*(C19–O7) | 0.096 | 62 | 1.652 | 0.341 |
| LP(1)O4 | 1.968 | σ*(N5–H) | 0.042 | 16 | 3.068 | 0.160 |
| LP(1)N5 | 1.706 | RY* C11 | 0.006 | 136 | 0.340 | 0.351 |
| σ(N5–H) | 1.983 | σ*(C11–C17) | 0.021 | 500 | 3.095 | 0.168 |
| σ(N3–H) | 1.990 | σ*(N1–C15) | 0.013 | 18 | 3.357 | 0.126 |

Occupancy of natural orbitals (NBOs) and hybrids calculated for 2-[(1H-benzimidazol-2-yl-methyl)-amino]-benzoic acid methyl ester (selected)

| Donor[a] Lewis-type NBOs (A–B) | Occupancy | Hybrid[e] | AO (%)[f] | Acceptor[b] non Lewis NBOs | NBOs |
|---|---|---|---|---|---|
| σ(C19–O7) | 1.992 | $sp^{2.68}d^{0.01}$ (C19)<br>$sp^{2.04}$ (O7) | s(27.09)p(72.65)d(0.26)<br>s(32.92)p(67.02) | σ*(C19–O7) | 0.0968 |
| σ(C19–O4) | 1.996 | $sp^{2.03}$ (C19)<br>$sp^{1.43}d^{0.01}$ (O4) | s(32.95)p(66.93)<br>s(41.03)p(58.62)d(0.35) | σ*(C19–O4) | 0.0186 |
| π(C19–O4) | 1.982 | $sp^{1.00}$ (C19)<br>$sp^{1.43}d^{0.01}$ (O4) | s(0.00)p(99.80)<br>s(0.00)p(99.69) | π*(C19–O4) | 0.3008 |
| σ(C21–O7) | 1.991 | $sp^{3.97}d^{0.01}$ (C21)<br>$sp^{2.54}$ (O7) | s(20.06)p(79.67)d(0.27)<br>s(28.21)p(71.72) | σ*(C21–O7) | 0.0142 |
| LP(1)N1 | 1.915 | $sp^{2.10}$ | s(32.23)p(67.20) | RY*(1)N1 | 0.0027 |
| LP(1)N3 | 1.632 | $sp^{1.00}$ | s(0.00)p(99.99) | RY*(1)N3 | 0.0018 |
| LP(1)O7 | 1.963 | $sp^{1.57}$ | s(38.85)p(61.09) | RY*(1)O7 | 0.0021 |
| LP(1)O4 | 1.968 | $sp^{0.71}$ | s(58.49)p(41.46) | RY*(1)O4 | 0.0015 |
| LP(1)N5 | 1.706 | $sp^{1.00}$ | s(0.00)p(99.99) | RY*(1)N5 | 0.0045 |

[a] LP(n)A is a valence lone pair orbital (n) on A atom.
[b] Starred label (*) denotes antibonding, and Ry corresponds to the Rydberg NBO orbital.
[c] Energy difference between donor and acceptor $i$ and $j$ NBO orbitals.
[d] $F(i,j)$ is the Fock matrix element between $i$ and $j$ NBO orbitals.
[e] Hybrid on A atom in the A–B bond or otherwise, as indicated.
[f] Percentage contribution of atomic orbitals in NBO hybrid.

level in order to elucidate the intramolecular, re-hybridization and delocalization of electron density within the molecule. The most important interactions between "filled" (donors) Lewis-type NBOs and "empty" (acceptors) non-Lewis NBOs are reported in Table 2. The electron density of six-conjugated single bond of aromatic ring (~1.6$e$) clearly demonstrates strong delocalization. The strong intramolecular hyperconjugative interaction of the σ electron of (N5–H) shares out to σ*(C11–C17) leading to stabilization of $\sim 3 \times 10^3$ kJ mol$^{-1}$. On the other hand, the π(C8–C10) in the benzimidazole ring further conjugate to the anti-bonding orbital of π*(C2–C9) and π*(C6–C12) which leads to strong delocalization with a considerable energy difference ~700 kJ mol$^{-1}$. The lone pair interaction of LP O7 with anti-bonding π*(C19–O4) has a large energy difference ($\sim 3.96 \times 103$ kJ mol$^{-1}$) which is an evidence for charge transfer from oxygen atom of the carbonyl group to the σ*(C19–O7).

Moreover, three classes of NBOs are included in Table 2, the Lewis-type (s and p bonding or lone pair) orbitals, the valence non-Lewis (acceptors, formally unfilled) orbitals and the Rydberg NBOs, which originate from orbitals outside the atomic valence shell. The calculated natural hybrids on atoms are also given in this Table 2. Table 1 collects the natural charges on atoms. The largest negative charges are located on the two $N_5$ (−0.611$e$) and $O_4$ (−0.628$e$). This can be interpreted in terms of intramolecular hydrogen bond, which formed through the latter atoms. The results from NBO analysis show that σ(C19–O7) is from $sp^{2.68}d^{0.01}$ hybrid on C19 (which is a mixture of 27.09% s, 72.56% p and 0.26% d atomic orbitals) and $sp^{2.04}$ on O7 (67.02% p contribution).

### 3.2.3. Frontier molecular orbitals

The frontier molecular orbitals play an important role in the electric and optical properties [28]. Fig. 3 shows the distributions and energy levels of the HOMO − 1, HOMO, LUMO and LUMO + 1 orbitals computed at the B3LYP/6-31G(d) level for our benzimidazole derivative. The value of the energy separation between the HOMO and LUMO is 4.39 eV.

## 3.3. Vibrational analysis

The theoretical IR spectrum of the title compound was obtained at DFT/B3LYP level of theory using 6-31G(d) basis set. All band assignments are presented in Table 3. At this level, the calculated harmonic force constants and frequencies are higher than the corresponding experimental quantities, due to basis set truncation and neglecting of electron correlation and mechanical anharmonicity [29]. To compensate these shortcomings, scale factors were introduced and an explanation of this approach was discussed [30]. Two different methods were applied: (i) *uniform* scaling [30], the scaling factor is 0.963 for 6-31G(d) basis set (ii) *linear regression method* [31]; in this method, the plot of the calculated frequencies versus their experimental values resulted in a straight line, whose equation was used to correct the calculated frequencies ($\nu_{calc}$).

**Table 3**
Observed and calculated selected frequencies ($cm^{-1}$) and assignments of the fundamental modes for 2-[(1H-benzimidazol-2-yl-methyl)-amino]-benzoic acid methyl ester.

| No. | Exp. Freq. | Calculated un-scaled frequency | Scaled frequency | | Vibrational assignments |
|---|---|---|---|---|---|
| | | | Uniform scaling | Linear regression scaling | |
| 1 | | 3648 | 3513 | 3503 | $\nu$ $NH^{ss}$/Bz |
| 2 | 3345 | 3495 | 3365 | 3356 | $\nu$ $NH^{ss}$/An |
| 3 | | 3237 | 3117 | 3108 | $\nu$ $CH^{ss}$/An |
| 4 | | 3220 | 3100 | 3092 | $\nu$ $CH^{ss}$/Bz |
| 5 | | 3218 | 3098 | 3090 | $\nu$ $CH^{ass}$/An |
| 6 | | 3208 | 3089 | 3080 | $\nu$ $CH^{ass}$/Bz |
| 7 | | 3207 | 3088 | 3079 | $\nu$ $CH^{ass}$/An |
| 8 | | 3196 | 3077 | 3069 | $\nu$ $CH^{ass}$/Bz |
| 9 | | 3186 | 3068 | 3059 | $\nu$ $CH^{ass}$/Bz |
| 10 | | 3182 | 3064 | 3055 | $\nu$ $CH^{ass}$/An |
| 11 | | 3176 | 3058 | 3049 | $\nu$ $CH_3{}^{ass}$ |
| 12 | 2987 | 3146 | 3029 | 3021 | $\nu$ $CH_3{}^{ass}$ |
| 13 | 2950 | 3076 | 2962 | 2953 | $\nu$ $CH_3{}^{ss}$ |
| 14 | | 2969 | 2859 | 2851 | $CH_2{}^{ass}$ |
| 15 | 2831 | 2961 | 2851 | 2843 | $CH_2{}^{ss}$ |
| 16 | 1674 | 1761 | 1695 | 1690 | $\nu$ CC/An + $\nu$ C = O + β NH/An |
| 17 | | 1684 | 1621 | 1616 | $\nu$ CC/Bz + β NH/Bz + $\nu$ C = N/Bz |
| 18 | | 1667 | 1605 | 1600 | $\nu$ CC/An + $\nu$ C = O |
| 19 | 1581 | 1642 | 1581 | 1576 | $\nu$ C = N/Bz + β NH/Bz |
| 20 | | 1626 | 1565 | 1560 | $\nu$ CC/An + β NH/An |
| 21 | | 1602 | 1542 | 1537 | $\nu$ CC/Bz + β NH/Bz + $\nu$ C = N/Bz + $\delta_s CH_2$ + β NH/An |
| 22 | 1512 | 1572 | 1513 | 1509 | $\delta_s CH_2$ + $\nu$ CC/An + β NH/An |
| 23 | | 1541 | 1483 | 1479 | $\delta_s CH_2$ |
| 24 | | 1535 | 1478 | 1473 | $\nu$ CC/Bz + $\delta_s CH_2$ |
| 25 | | 1525 | 1468 | 1463 | $CH_3{}^{opb}$ |
| 26 | 1447 | 1511 | 1455 | 1450 | $CH_3{}^{ipb}$ |
| 27 | | 1493 | 1437 | 1433 | $CH_3{}^{sb}$ + β NH/An + ω $CH_2$ + $\nu$ CC/An |
| 28 | | 1458 | 1404 | 1399 | $\nu$ CC/An + $\nu$ CC/Bz + β NH/An + ω $CH_2$ + β NH/Bz + $\nu$ C-NH/Bz |
| 29 | | 1429 | 1376 | 1371 | $\nu$ CC/An + $\nu$ CC/Bz + β NH/An + ω $CH_2$ + β NH/Bz + β CH/An + β CH/Bz |
| 30 | 1323 | 1371 | 1320 | 1316 | $\nu$ CC/An + β NH/An + β CH/An |
| 31 | | 1325 | 1275 | 1271 | β CH/An + β CH/Bz + ω $CH_2$ |
| 32 | | 1302 | 1253 | 1249 | β CH/Bz + $\nu$ CC/Bz |
| 33 | 1235 | 1298 | 1249 | 1245 | β NH/An + β CH/An |
| 34 | | 1257 | 1210 | 1206 | β CH/Bz |
| 35 | | 1256 | 1209 | 1172 | τ$CH_2$ |
| 36 | | 1222 | 1176 | 1161 | $CH_3{}^{opr}$ |
| 37 | | 1210 | 1165 | 1149 | $\nu$ C-NH/An + β CH/An + β NH/Bz + β CH/Bz |
| 38 | 1159 | 1198 | 1153 | 1205 | β NH/An |
| 39 | | 1185 | 1141 | 1137 | $CH_3{}^{ipr}$ |
| 40 | | 1182 | 1138 | 1134 | β CH/Bz |
| 41 | | 1155 | 1112 | 1108 | β CH/An + $CH_2$-NH/An + $\nu$ C–O–$CH_3$ + β NH/Bz |
| 42 | 1115 | 1154 | 1112 | 1096 | $CH_3{}^{ipr}$ |
| 43 | 1073 | 1142 | 1099 | 1038 | β CH/Bz |
| 44 | 1024 | 1082 | 1041 | 1001 | β CH/An |
| 45 | | 1044 | 1005 | 1108 | $\nu$ $(CC)_{Bz}$ boat shape |
| 46 | | 999 | 962 | 958 | $\nu$ C–O–$CH_3$ + $\nu$ CC/An |
| 47 | | 1043 | 1004 | 1000 | ρ$CH_2$ |
| | | 672 | 647 | 644 | |
| 48 | 909 | 1023 | 985 | 981 | Rtorsion/Bz |
| 49 | 702 | 976 | 939 | 936 | γ CH/An |
| | 660 | 955 | 919 | 916 | |
| | | 844 | 812 | 809 | |
| | | 763 | 734 | 731 | |
| | | 761 | 732 | 730 | |
| | | 707 | 680 | 678 | |
| | | 536 | 516 | 513 | |
| | | 447 | 430 | 428 | |
| 50 | | 911 | 877 | 874 | Rtorsion/Bz |
| | | 974 | 937 | 934 | |
| | | 930 | 895 | 892 | |
| 51 | 870 | 860 | 828 | 825 | γ CH/Bz |
| | 749 | 776 | 747 | 744 | |
| | 528 | 756 | 728 | 725 | |
| | | 588 | 566 | 563 | |
| | | 438 | 421 | 419 | |
| 52 | | 829 | 798 | 795 | β $(COO)_{ss}$ |
| 53 | | 632 | 608 | 606 | Rtrigd/Bz |
| 54 | | 680 | 654 | 652 | Rtorsion/An |
| 55 | | 636 | 612 | 609 | γ NH/An |
| 56 | | 417 | 401 | 399 | γ NH/Bz |
| 57 | | 258 | 249 | 246 | τ$CH_3$ |

R: ring; ss: symmetric stretching; ass: asymmetric stretching; $\nu$, stretching; β, in-plane bending; γ, out-of-plane bending; ρ, rocking; ω, wagging; τ, torsion; trig: trigonal; trigd: trigonal deformation. ops: out-of-plane stretching; sb: symmetric bending; ipb: in-plane-bending; opb: out-of-plane bending; ipr: in plane-rocking; opr: out-of-plane rocking.

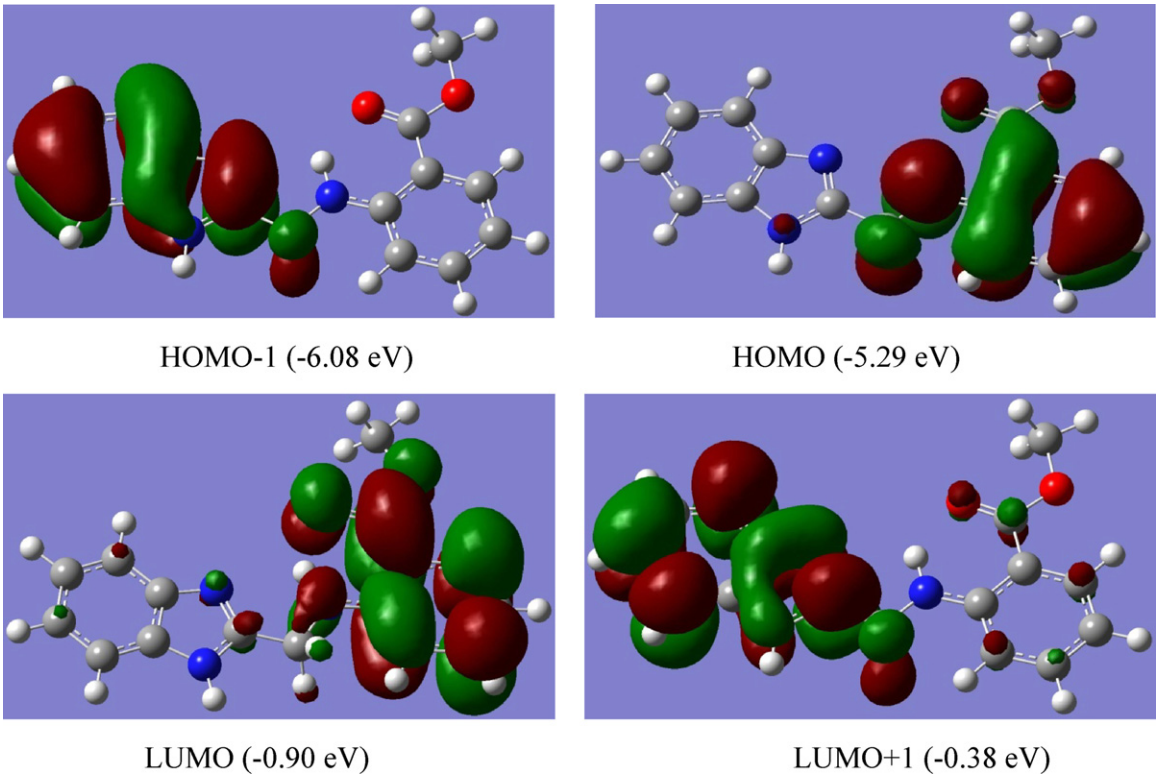


**Fig. 3.** Molecular orbital surfaces and energy levels of 2-[(1H-benzimidazol-2-ylmethyl)-amino]-benzoic acid methyl ester.

The title molecule has a strong inter- and intramolecular hydrogen bonds in the solid state, which makes the IR spectrum shows strong and broad absorption band in the region 3500–2200 $cm^{-1}$. Thus, it is difficult to assign the benzimidazolic NH band ($NH_{Bz}$). By using B3LYP/6-31G(d) method, the scaled calculated value at 3513 $cm^{-1}$ is assigned to $\nu(NH_{Bz})$. The sharp band at 3345 $cm^{-1}$ is assigned to $\nu(NH_{sec})$ with deviation from the theoretically scaled value by 20 $cm^{-1}$. This discrepancy may be justified on the basis that the calculations were performed on a single molecule in the gaseous state contrary to the experimental values, which were recorded in presence of intra-molecular interactions. The stretching mode of C=N group is overlapped with the aromatic C=C and C=O bands under the effect of the intermolecular hydrogen bond, whereas its theoretical value is found at 1667 $cm^{-1}$ that is in agreement with that previously reported [32]. The band at 1674 $cm^{-1}$ is assigned to the stretching mode of the carbonyl group beneath the effect of the intramolecular hydrogen bond and resonance.

Theoretically, the benzimidazole derivative gives rise to eight C–H aromatic stretching mode of vibration corresponding to the presence of eight aromatic C–H bonds as shown in Table 3. For assignments of $CH_3$ group frequencies theoretically, nine fundamentals can be associated to each $CH_3$ group [27]. The bands observed at 3058, 3029, and 2962 $cm^{-1}$ are ascribed to $CH_3$ asymmetric and symmetric stretching vibration. Infrared bands established at 1468, 1455, 1437, 1176, 1141 and 249 $cm^{-1}$ are attributed to $CH_3{}^{opb}$, $CH_3{}^{ipb}$, $CH_3{}^{sb}$, $CH_3{}^{opr}$, $CH_3{}^{ipr}$, and $\tau CH_3$ vibration mode, respectively. The RMS error of the frequencies between the un-scaled and experimentally observed in our compound was found to be 86 $cm^{-1}$. After scaling, the RMS error is found to be 13 $cm^{-1}$.

### 3.4. $^{13}C$ and $^{1}H$ NMR spectral analysis

In order to provide an unambiguous assignment of $^{13}C$ and $^{1}H$ NMR spectra of the studied compound, we undertook a series of NMR calculations using GIAO approximation, and the results of these calculations are shown in Table 4. The default IEF–PCM model provided by GAUSSAIN 03 was also tested in order to describe the influence exerted by solvent on the NMR spectra of the given compound. Results of linear regression fit between experimental and calculated chemical shifts ($^{1}H$ and $^{13}C$) performed for the structure tested are also included in Table 4. The $^{1}H$ chemical shifts of all protons in a given compound except the hydrogen-bonded one ($H_3$ and $H_5$) are in a good agreement with the theoretically computed values as shown in Table 4. The regression coefficient between the calculated and experimental chemical shifts is improved in presence of DMSO as a solvent. It was observed that the chemical shifts are slightly increased in water as compared with those obtained in DMSO.

The title molecule showed a broad singlet signal in DMSO at 12.35 ppm [9] due to the benzimidazolic NH proton ($H_3$). This proton is shifted towards higher magnetic field than the calculated one by 3.37 ppm in case of DMSO and 4.40 ppm in the gaseous state as previously reported [33]. Thus, the inclusion of solvent in this case increases the shift by 1.03 ppm in DMSO, which shows the importance of the use of solvation in shielding calculations. Moreover, the calculated chemical shift for the intermolecular H-bonding proton ($H_3$) in chloroform shows better agreement with the experimental value than that of DMSO as shown in Table 4 owing to the difference in polarity. The triplet signal at 8.30 ppm is due to the secondary amino group that is lower than the calculated value by 1.21 ppm in DMSO and 1.65 ppm in gaseous state. Although, the calculated values of the hydrogen-bonded protons ($H_3$ and $H_5$) in the DMSO showed little improvement in relation to the gaseous state, but these values remain unacceptable apart from the experimental values, being obviously that chemical shifts associated with these protons are not correctly described by continuum model [34]. Thus, it is clear that continuum model fails in reproducing the experimental findings for the hydrogen-bonded protons (N3 & N5) and specific solute–solvent interactions are expected to

**Table 4**
Experimental and calculated $^{1}H$ and $^{13}C$ NMR chemical shifts for title compound.

| Atom | δ Calcd. | | | | δ Exp. |
|---|---|---|---|---|---|
| | Gaseous | DMSO | Water | $CHCl_3$ | DMSO |
| $H_3$ | 7.95 | 8.98 | 9.00 | 9.42 | 12.35 |
| $H_5$ | 9.95 | 9.51 | 9.53 | 10.36 | 8.30 |
| $H_8$ | 7.53 | 7.69 | 7.69 | 7.67 | 7.15 |
| $H_9$ | 8.14 | 8.05 | 8.05 | 8.09 | 7.58 |
| $H_{10}$ | 7.50 | 7.73 | 7.73 | 7.67 | 7.14 |
| $H_{12}$ | 7.55 | 7.82 | 7.82 | 7.70 | 7.40 |
| $H_{13}$ | 4.59 | 4.87 | 4.87 | 4.77 | 4.68 |
| $H_{14}$ | 7.65 | 7.91 | 7.91 | 7.82 | 7.35 |
| $H_{17}$ | 6.78 | 6.96 | 6.97 | 6.84 | 6.76 |
| $H_{18}$ | 8.56 | 8.48 | 8.48 | 8.46 | 7.83 |
| $H_{20}$ | 6.63 | 6.96 | 6.96 | 6.91 | 6.64 |
| $H_{21}$ | 3.89 | 4.03 | 4.03 | 4.01 | 3.80 |
| $R^2$ | 0.9759 | 0.9929 | 0.9932 | 0.9886 | |
| $C_2$ | 152.2 | 149.4 | 149.4 | 149.8 | 134.7 |
| $C_6$ | 141.7 | 141.7 | 141.7 | 141.3 | 134.6 |
| $C_8$ | 127.5 | 126.4 | 126.4 | 126.6 | 115.1 |
| $C_9$ | 125.5 | 123.6 | 123.5 | 124.5 | 115.0 |
| $C_{10}$ | 128.6 | 128.2 | 128.2 | 128.1 | 120.0 |
| $C_{11}$ | 157.0 | 156.2 | 156.2 | 156.3 | 150.0 |
| $C_{12}$ | 112.5 | 114.3 | 114.3 | 113.2 | 110.0 |
| $C_{13}$ | 44.4 | 44.1 | 44.1 | 44.1 | 51.5 |
| $C_{14}$ | 140.6 | 141.2 | 141.2 | 141.3 | 131.1 |
| $C_{15}$ | 140.6 | 157.4 | 157.5 | 156.3 | 150.1 |
| $C_{16}$ | 115.4 | 115.9 | 115.8 | 116.3 | 152.4 |
| $C_{17}$ | 113.7 | 115.1 | 115.2 | 114.4 | 110.1 |
| $C_{18}$ | 139.4 | 138.3 | 138.2 | 138.5 | 120.1 |
| $C_{19}$ | 182.2 | 178.0 | 178.1 | 177.6 | 167.5 |
| $C_{20}$ | 118.0 | 118.0 | 118.0 | 117.8 | 111.6 |
| $C_{21}$ | 56.5 | 53.6 | 53.7 | 53.5 | 60.1 |
| $R^2$ | 0.9525 | 0.9767 | 0.9770 | 0.9748 | |

completely explain the NMR spectra of the studied compound [34]. Thus, the GIAO method showed significant differences in chemical shifts between the hydrogen-bonding protons and non-hydrogen-bonding protons.

More structural information about the target compound was provided by the $^{13}C$ NMR spectrum. The chemical shifts at 51.5 (theoretical value = 44.4 ppm) and 60.1 ppm (56.5 ppm) are assigned to $CH_2$ and $OCH_3$, respectively. The signal at 167.5 ppm is attributed to C=O (theoretical value = 182.2 ppm). The theoretical $^{13}C$ results were in remarkably good agreement with the experimental values, with mean absolute error (MAE) does not exceed 10 ppm for all carbons except the carbonyl group. This may be due to intramolecular hydrogen bond, which has not been in our calculations. The carbons are less affected by external influence and the calculated values show an excellent correlation with the experimental values. The regression coefficient between the calculated and experimental chemical shifts was 0.9767 for $^{13}C$ NMR data in DMSO. The high linear correlation coefficients ($R^2$) and low MAE value established the robustness of the assignments.

### 3.5. Electronic absorption

#### 3.5.1. Band assignment

The electronic spectrum of 2-[(1H-benzimidazol-2-ylmethyl)-amino]-benzoic acid methyl ester displayed six absorption bands in ethanol at 203, 225, 250, 273, 280 and 342 nm as shown in Fig. 4. The first two bands may be assigned to medium and low energy $\pi$–$\pi^*$ transitions within the phenyl rings of the aniline and benzimidazole moieties, respectively [35]. In benzimidazole ring, three kinds of transitions are possible: (i) $n$–$\pi^*$, (ii) $\pi$–$\pi^*$, and (iii) charge–transfer. However, it is well established that the $n$–$\pi^*$ transition is not observed in the benzimidazole compounds, although the system has a lone pair of electrons on the tertiary nitrogen atom [36]. Therefore, the bands at 250, 273, and 280 nm may be assigned to $\pi$–$\pi^*$ transitions in the benzimidazole ring. In addition, the bands at 273 and 280 nm appear doublet due to the probable existence of a tautomeric structure [37]. This phenomenon is supported by comparing our spectrum with the spectrum of 1-methyl-2-phenyl-benzimidazole [36], where this fine structure is lost. The geometry of the title compound suggests the formation of intramolecular hydrogen bond. This hydrogen bond will force the lone pair of the carbonyl group to be parallel with the $\pi$-cloud and thereby increases the resonance character of this group with the aniline moiety [38]. This results in the appearance of a band at 342 nm.

The absorption spectrum of our compound was observed in solvents of different polarity and of hydrogen bond formation tendency (Fig. 4). The two bands at 274 and 280 nm in the cylcohexane (reference solvent) are slightly blue shifted in ethanol and 2-propanol (hydrogen-bonding solvents) suggests that the benzimidazole derivative is acting as a proton acceptor [39] at the pyridine-type nitrogen. However, the latter bands are red-shifted in DMF and DMSO (hydrogen bond acceptor solvents) due to an almost proton transfer from the solute molecules to these solvents. The values of the observed transition energies ($E_{obs}$) and oscillator strengths ($f_{obs}$) of all the bands in the electronic spectra of the title compound in different solvents were calculated [35] and tabulated in Supplementary Material, Table S2.

Theoretical UV/vis. spectrum of 2-methylbenzimidazole [40] in the gaseous state is characterized by three bands at 202, 238 and 251 nm and the absorptions are basically the $\pi$–$\pi^*$ type. Direct attachment of aniline moiety to the 2-methylbenzimidzole ring produces a bathochromic shift, 212, 244, and 253 nm, with additional bands at 261 and 323 nm. The bathochromic shift observed can be attributed to an increase in the length of a conjugated system. As the extent of conjugation increases, the magnitude of the bathochromic shift also increases due to the stabilization of the aromatic moiety. The calculated excitation energies

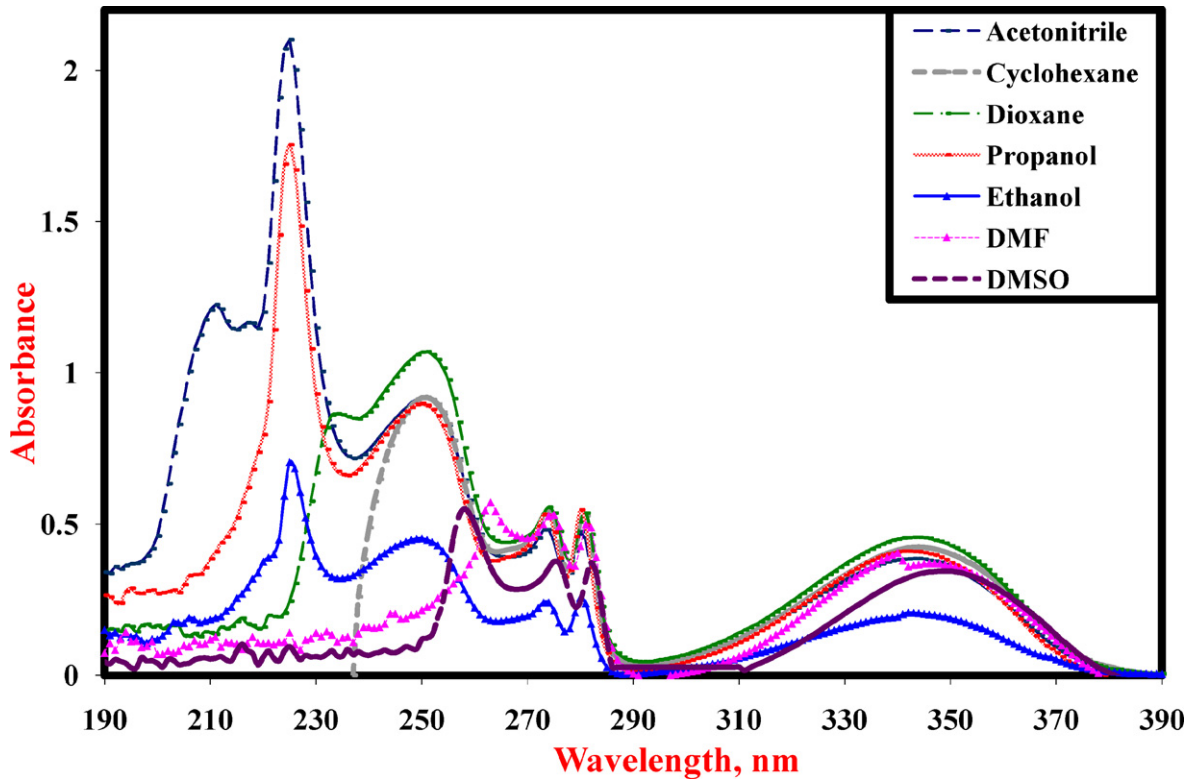


**Fig. 4.** Electronic absorption spectra of $3 \times 10^{-5}$ M of title compound in different solvents (acetonitrile, cyclohexane, dioxane, DMSO, 2-propanol, ethanol and DMF).

are underestimated by 6–20 nm with respect to those obtain experimentally as the non-specific solute–solvent interactions (in the gas phase), have not been considered in the calculations.

*3.5.2. Electronic absorption spectra in solutions of varying pH*

The absorption spectra of $3 \times 10^{-5}$ M solutions of our compound in 20% (v/v) ethanolic solutions of varying pH values were scanned in the UV/vis. range. The bands located at 250, 274 and 280 nm in ethanol are blue shifted to 243, 269 and 275 nm at pH 2 ($H_2L^{2+}$). With increasing the pH, these bands remain in their new positions with appearance of shoulder at 279 nm at pH 5. Between pH 6 and 12, these bands are red shifted to 247, 273, and 279 nm, accompanied by a variation in the absorbance values according to the presented species ($L^-$ and $L^{2-}$). This compound possesses a clear isosbestic point in the acidic medium (pH = 2–6) at 209 nm corresponding to the equilibrium between the dication and monocation species. The pH-absorbance changes [35] were utilized to calculate the acid dissociation constants. Four p$K_a$ values were reported. The first one is $3.42 \pm 0.03$ corresponding to deprotonation of the protonated secondary amino group. The p$K_a$ value $4.72 \pm 0.01$ may be attributed to the ionization of the protonated pyridine

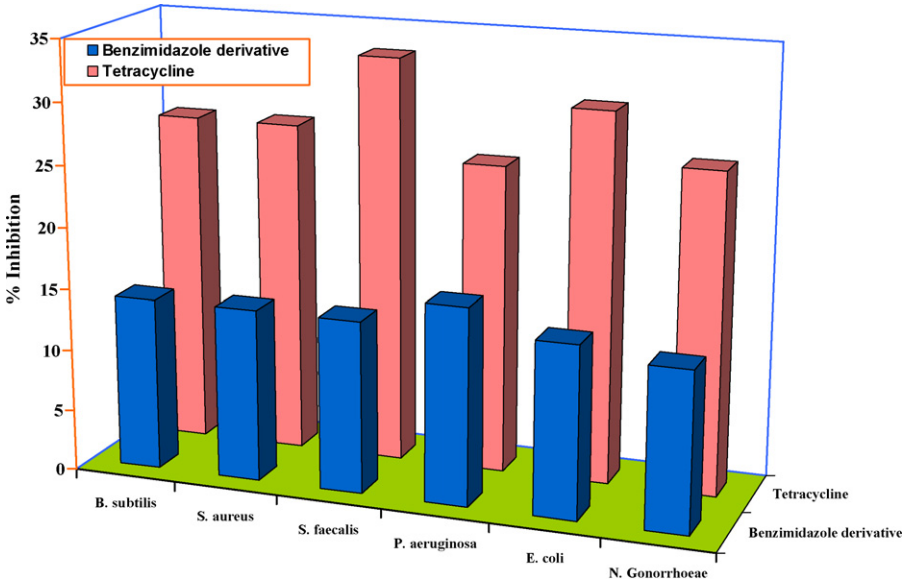


**Fig. 5.** Antibacterial activities of benzimidazole L against *B. subtilis*, *S. aureus*, *S. faecalis* as Gram-positive, *P. aeruginosa*, *E. coli*, *N. Gonorrhoeae* as Gram-negative bacteria.

type nitrogen [41]. The third p$K_a$ (9.62 ± 0.02) is accounted for the ionization of the $NH_{sec}$ group, while the fourth p$K_a$ (11.00 ± 0.03) is attributed to deprotonation of the imidazolic proton.

### 3.6. Biological activity

The antimicrobial activities were carried out using cultures of *B. subtilis*, *S. aureus*, and *S. faecalis* as Gram-positive bacteria and *E. coli*, *P. aeruginosa*, and *N. gonorrhoeae* as Gram-negative bacteria. The data showed that the title compound has the capacity of inhibiting the metabolic growth of the investigated bacteria to different extents (Fig. 5). The remarkable activity of this compound may be arising from the benzimidazole ring, which may play an important role in the antibacterial activity. The mode of action may involve formation of hydrogen bond through the pyridine-type nitrogen and/or the carbonyl group with the active centers of the cell constituents, resulting in interference with the normal cell process. A possible explanation for the lower activity of this compound with respect to tetracycline may be due its low lipophilicity, where the penetration through the lipid membrane is decreased and hence, they cannot block or inhibit the growth of the microorganism.

## 4. Conclusion

In an effort to prepare a new compound with potential biological activity, we have synthesized and characterized 2-[(1H-benzimidazol-2-yl-methyl)-amino]-benzoic acid methyl ester by X-ray crystallography, elemental analysis, $^1H$, $^{13}C$ NMR, UV/vis., and FT-IR spectroscopy. The comparisons of the DFT calculations with the crystal structure and the vibrational and NMR spectra showed excellent agreement. The inclusion of solvation to NMR calculations proved to be very important in obtaining better values than in gaseous state, especially for acidic protons. The results showed that the title compound has the capacity of inhibiting the metabolic growth of the investigated bacteria to different extents.

## Supplementary Material

CCDC 721702 contains the supplementary crystallographic data for this paper. These data can be obtained free of charge via www.ccdc.cam.ac.uk/conts/retrieving.html (or from the Cambridge Crystallographic Data Center, 12, Union Road, Cambridge CB2 1EZ, UK; fax: +44 1223 336033).

## Acknowledgment

We would like to extend our grateful thanks to Dr. Mohamed Elshakre, Chemistry Department, Faculty of Science, Cairo University for allowing us to use his version of the *GAUSSIAN 03* package of programs.

## Appendix A. Supplementary data

Supplementary data associated with this article can be found, in the online version, at doi:10.1016/j.saa.2011.07.021.

## References

[1] R.J. Sundberg, R.B. Martin, Chem. Rev. 74 (1974) 471–517.
[2] P.N. Preston, Chem. Rev. 74 (1974) 279–314.
[3] (a) V. Rajendiran, M. Murali, E. Suresh, S. Sinha, K. Somasundaram, M. Palaniandavar, Dalton Trans. (2008) 2157–2170;
(b) J. Mann, A. Baron, Y. Opoku-Boahen, E. Johansson, G. Parkinson, L.R. Kelland, S. Neidle, J. Med. Chem. 44 (2001) 138–144.
[4] N.M. Goudgaon, V. Dhondiba, A. Vijayalaxmi, Ind. J. Heterocycl. Chem. 13 (2004) 271–272.
[5] (a) S.J. Hsu, K.M. Hsu, M.K. Leong, I.J.B. Lin, Dalton Trans. (2008) 1924–1931;
(b) I. Dinarès, N. Mesquida, ARKIVOC 4 (2007) 408.
[6] (a) W. Xie, Y. Zhao, C. Li, S. Liu, Solid-State Electron. 51 (2007) 1129–1132;
(b) Z. Ge, T. Hayakawa, S. Ando, M. Ueda, T. Akiike, H. Miyamoto, T. Kajita, M.A. Kakimoto, Chem. Mater. 20 (2008) 2532–2537;
(c) G. Schwartz, K. Fehse, M. Pfeiffer, K. Walzer, K. Leo, Appl. Phys. Lett. 89 (2006) 83509.
[7] L. Li, G.J. Clarkson, Org. Lett. 9 (2007) 497–500.
[8] (a) H.C. Yao, M.M. Li, G.S. Yang, Z.J. Li, Y. Zhu, Inorg. Chim. Acta 360 (2007) 3959–3964;
(b) L. Wei, J.W. Babich, W. Ouellette, J. Zubieta, Inorg. Chem. 45 (2006) 3057–3066;
(c) M. Huang, P. Liu, J. Wang, Y. Chen, Z. Liu, Q. Liu, Inorg. Chem. Commun. 9 (2006) 952–954;
(d) C.K. Lee, K.M. Hsu, C.H. Tsai, C.K. Lai, I.J.B. Lin, Dalton Trans. (2004) 1120–1126;
(e) K. Isele, V. Broughton, C.J. Matthews, A.F. Williams, G. Bernardinelli, P. Franz, S. Decurtins, Dalton Trans. (2002) 3899–3905.
[9] N.T. Abdel-Ghani, A.M. Mansour, J. Mol. Struct. 991 (2011) 108–126.
[10] (a) S.M. Mayanna, T.H.V. Setty, Corrosion Sci. 15 (1975) 625–631;
(b) R. Walker, Anti-Corrosion 17 (1970) 9;
(c) F. Mansfeld, T. Smith, E.P. Perry, Corrosion 27 (1971) 289–294.
[11] N.T. Abdel-Ghani, A.M. Mansour, Inorg. Chim. Acta 373 (2011) 249–258.
[12] (a) J. Phillips, Chem. Soc. (1928) 2393;
(b) H. Skolnik, J. Miller, A.R. Day, J. Am. Chem. Soc. 65 (1943) 1854–1862.
[13] (a) A.D. Becke, J. Chem. Phys. 98 (1993) 5648–5682;
(b) C. Lee, W. Yang, R.G. Parr, Phys. Rev. B. 37 (1998) 785–789.
[14] M.J. Frisch, G.W. Trucks, H.B. Schlegel, G.E. Scuseria, M.A. Robb, J.R. Cheeseman, V.G. Zakrzewski, J.A. Montgomery, R.E. Stratmann, J.C. Burant, S. Dapprich, J.M. Millam, A.D. Daniels, K.N. Kudin, M.C. Strain, O. Farkas, J. Tomasi, V. Barone, M. Cossi, R. Cammi, B. Mennucci, C. Pomelli, C. Adamo, S. Clifford, J. Ochterski, G.A. Petersson, P.Y. Ayala, Q. Cui, K. Morokuma, D.K. Malick, A.D. Rabuck, K. Raghavachari, J.B. Foresman, J. Cioslowski, J.V. Ortiz, A.G. Baboul, B.B. Stefanov, G. Liu, A. Liashenko, P. Piskorz, I. Komaromi, R. Gomperts, R.L. Martin, D.J. Fox, T. Keith, M.A. Al-Laham, C.Y. Peng, A. Nanayakkara, C. Gonzalez, M. Challacombe, P.M.W. Gill, B.G. Johnson, W. Chen, M.W. Wong, J.L. Andres, M. Head-Gordon, E.S. Replogle, J.A. Pople, GAUSSIAN 03 (Revision A.9), Gaussian, Inc., Pittsburgh, 2003.
[15] A. Frisch, A.B. Nielson, A.J. Holder, GAUSSVIEW User Manual , Gaussian Inc, Pittsburgh, PA, 2000.
[16] R. Ditchfield, Chem. Phys. 76 (1972) 5688–5691.
[17] A.L. Spek, J. Appl. Cryst. 36 (2003) 7–13.
[18] A.L. Spek, Program for Reduction of CAD-4 Data , University of Utrecht, The Netherlands, 1996.
[19] A. Altomare, G. Cascarano, C. Giacovazzo, A. Guagliardi, M.C. Burla, G. Polidori, M. Camalli, J. Appl. Cryst. 27 (1994) 435–436.
[20] S. Mackay, C.J. Gilmore, C. Edwards, N. Stewart, K. Shankland, Maxus Computer Program for the Solution and Refinement of Crystal Structures , MacScience, Japan & The University of Glasgow, Bruker Nonius, The Netherlands, 1999.
[21] C.K. Johnson, ORTEP–II. A Fortran Thermal–Ellipsoid Plot Program. Report ORNL-5138 , Oak Ridge National Laboratory, Oak Ridge, TN, USA, 1976.
[22] (a) D. Greenwood, Antimicrobial Chemotherapy. Part II. Laboratory Aspects of Antimicrobial Therapy , Bailliere, Tindall, London, 1983, p. 71;
(b) V. Lorian, Antibiotics in Laboratory Medicine , Williams & Wilkins, Baltimore, 1996.
[23] National Committee for Clinical Laboratory Standards, NCCLS Approval Standard Document M2-A7, Vilanova, PA, 2000.
[24] A.E. Reed, L.A. Curtiuss, F. Weinhold, Chem. Rev. 88 (1988) 899–926.
[25] (a) U.P. Salzner, V.R. Schleyer, J. Am. Chem. Soc. 115 (1993) 10231–10236;
(b) U. Salzner, P.V.R. Schleyer, J. Org. Chem. 59 (1994) 2138–2155;
(c) H. Roohi, A. Ebrahimi, J. Mol. Struct.: Theochem. 726 (2005) 141–148.
[26] H. Roohi, A. Ebrahimi, F. Alirezapoor, M. Hajealirezahi, Chem. Phys. Lett. 409 (2005) 212–218.
[27] C. Ravikumar, I. Hubert Joe, V.S. Jayakumar, Chem. Phys. Lett. 460 (2008) 552–558.
[28] I. Fleming, Frontier Orbitals and Organic Chemical Reactions , Wiley, London, 1976.
[29] (a) G. Rauhut, P. Pulay, J. Phys. Chem. 99 (1995) 3093–3100;
(b) J.A. Pople, H.B. Schlegel, R. Krishnan, J.S. Defrees, J.S. Binkley, M.J. Frisch, R.A. Whiteside, Int. J. Quantum Chem.: Quantum Chem. Symp. 15 (1981) 269–278.
[30] (a) M.W. Ellzy, J.O. Jensen, H.F. Hameka, J.G. Kay, D. Zeroka, Spectrochim. Acta 57A (2001) 2417–2432;
(b) J.O. Jensen, A. Banerjee, C.N. Merrow, D. Zeroka, J.M. Lochner, J. Mol. Struct.: Theochem. 531 (2000) 231–323;
(c) J.O. Jensen, D. Zeroka, J. Mol. Struct.: Theochem. 487 (1999) 267–274.
[31] O. Sala, N.S. Goncalves, L.K. Noda, J. Mol. Struct. 411 (2001) 565–566.
[32] (a) S. Mohan, N. Sundaraganesan, Spectrochim. Acta A 47 (1991) 1111–1115;
(b) N. Sundaraganesan, S. Ilakiamani, P. Subramani, B. Dominic Joshua, Spectrochim. Acta Part A 67 (2007) 628–635.
[33] (a) E. Bednarek, J.C. Dobrowolski, K. Dobrosz-Teperek, L. Kozerski, W. Lewandowski, A.P. Mazurek, J. Mol. Struct. 554 (2000) 233–243;
(b) F.S. Miranda, F.G. Menezes, J. Vicente, A.J. Bortoluzzi, C.Z. Ademir-Neves, N.S. Gonçalves, J. Mol. Struct. 938 (2009) 1–9.
[34] V. Chiş, A. Pîrnău, M. Vasilescu, R.A. Varga, O. Oniga, J. Mol. Struct.: Theochem. 851 (2008) 63–74.
[35] R.M. Issa, A.A. Hassanein, I.M. El-Mehasseb, R.I. Abed El-Wadoud, Spectrochim. Acta Part A 65 (2006) 206–214.

[36] (a) M. Krishnamurthy, P. Phaniraj, S.K. Dogra, J. Chem. Soc. Perkin Trans. II (1986) 1917–1925 (and the references therein);
(b) A.K. Mishra, S.K. Dogra, J. Photochem. 31 (1985) 333–344;
A.K. Mishra, S.K. Dogra, Ind. J. Phys. Sect. B 54 (1984) 480;
A.K. Mishra, S.K. Dogra, Spectrochim. Acta Part A 39 (1983) 609–615.
[37] R.M. Issa, S.A. El-Daly, N.A. El-Wakiel, Spectrochim. Acta Part A 59 (2003) 723–728.
[38] J.K. Dey, S.K. Dogra, Bull. Chem. Soc. Jpn. 64 (1991) 3142–3152.
[39] P.N. Preston, Benzimidazoles and Congeneric Tricyclic Compounds, Part I , Wiley, New York, 1981, p. 64.
[40] R.I. Castillo, S.P.H. Rivera, J. Mol. Struct. 968 (2010) 6–12.
[41] A.K. Mishra, S.K. Dogra, Bull. Chem. Soc. Jpn. 58 (1985) 3587–3592;
A.K. Mishra, S.K. Dogra, J. Photochem. 31 (1985) 333–342;
A.K. Mishra, S.K. Dogra, Ind. J. Phys. Sect. B 54 (1984) 480–486;
A.K. Mishra, S.K. Dogra, Spectrochim. Acta Part A 39 (1983) 609–611.